GEODYNAMICS & TECTONOPHYSICS
Published by the Institute of the Earth's Crust, Siberian Branch, Russian Academy of Sciences

PALEOGEODYNAMICS

2024 VOLUME 15 ISSUE 3 ARTICLE 0756

ISSN 2078-502X

DOI: 10.5800/GT-2024-15-3-0756

# GEODYNAMICS AND ORE CONTENT OF PROTEROZOIC MAPHITES IN THE CENTRAL PART OF THE ALDAN-STANOVOY SHIELD (SOUTHERN NORTH ASIAN CRATON)

**A.A. Kravchenko** [1]✉, **A.V. Okrugin** [1], **V.I. Beryozkin**[1], **N.V. Popov**[2], **E.E. Loskutov** [1]

[1] Diamond and Precious Metal Geology Institute, Siberian Branch of the Russian Academy of Sciences, 39 Lenin Ave, Yakutsk 677007, Republic of Sakha (Yakutia), Russia

[2] Trofimuk Institute of Petroleum Geology and Geophysics, Siberian Branch of the Russian Academy of Sciences, 3 Academician Koptyug Ave, Novosibirsk 630090, Russia

**ABSTRACT.** The study of diverse mantle-derived igneous complexes is important for interpreting geodynamic events, ore deposits formation mechanisms, and ore-forming fluid sources. Modern studies of orogenic gold deposits in the Precambrian metamorphosed terranes emphasize the importance of subduction-enriched lithospheric mantle in the ore formation processes. Orogenic gold mineralization in the Nimnyr terrane of the Aldan-Stanovoy shield is confined to the outcrops of mafic granulites from the Medvedev complex, intruded and metamorphosed 1.92–1.90 Ga ago at the final stage of the collision process. The Medvedev complex and ore bodies are intersected by non-metamorphosed dolerites of the 1.87 Ga Timpton-Gynym and 1.75 Ga Timpton-Algamai dike belts formed under conditions of post-collisional and intracontinental extension. The mantle-derived igneous complexes, presenting in a variety of geodynamic settings and ore mineral formation stages, make it possible to identify compositional and evolutionary features of the mantle in connection with ore formation processes. To do this, there were determined rock-forming oxide and trace element concentrations in pre-ore mafic granulites of the Medvedev complex and post-ore dolerites. Based on the geochemical data, there was a reconstruction of rock and mantle source type formation conditions. It was found that the rocks of the Medvedev complex are plume-derived. Doleritic melt formation was contributed to by the subduction-enriched lithospheric mantle material. There is a possility of different degrees of source melting and interaction of plume with the enriched lithospheric mantle at the final stage of the collision process. The obtained results can be used to refine the geodynamic models of gold mineralization formation in the central part of the Aldan-Stanovoy shield. There has been proposed one of the standard models.

**KEYWORDS:** geodynamics; metallogeny; mantle magmatism; Proterozoic; Aldan shield

**FUNDING:** The research was carried out within DPMGI SB RAS research project 2024-0007. The research was coordinated with state assignment project FWZZ-2022-0002.

EDN: PAHHPA

**RESEARCH ARTICLE**

**Correspondence:** Alexander A. Kravchenko, kravchenkoaa@diamond.ysn.ru

Received: August 24, 2023
Revised: March 25, 2024
Accepted: April 15, 2024

**FOR CITATION:** Kravchenko A.A., Okrugin A.V., Beryozkin V.I., Popov N.V., Loskutov E.E., 2024. Geodynamics and Ore Content of Proterozoic Maphites in the Central Part of the Aldan-Stanovoy Shield (Southern North Asian Craton). Geodynamics & Tectonophysics 15 (3), 0756. doi:10.5800/GT-2024-15-3-0756

**Supplementary files:** Kravchenko_et_al_Suppl_1.xlsx

## 1. INTRODUCTION

The Paleoproterozoic accretionary and collisional structures (2.2–1.6 Ga) are characterized by the combination of pyrite-polymetallic, gold and copper-nickel-platinum-metallic ores [Turchenko, 2021]. The exposed Nimnyr terrane within the Aldan-Stanovoy Shield (Fig. 1) is no exception. The Precambrian geological complex terranes interpreted as the root zones of the Paleoproterozoic orogenic belt [Smelov, Timofeev, 2003] are known for the Precambrian metamorphogenic gold [Syasko et al., 2006] and skarn deposit with high Fe, Mn, Cu, and Co concentrations [Parfenov, Kuzmin, 2001]. The placer gold deposits often reveal a platinum-sperrylite association. Thus, the Unga-Nimgerkan placer deposits are characterized by the presence of rounded sperrylite grains, often with a thin surface coating of native platinum, which contain small kaolinite, pyrophyllite, endellite, phlogopite, ore mineral and quartz inclusions. The studies of structural features and mineral inclusions showed that such intergrowths were formed during thermal metamorphic decomposition of sperrylite at temperatures between 400 and 600 °C with participation of hydroxyl-containing minerals [Okrugin, 2000]. The $^{190}$Pt-$^{4}$He age of three sperrylite grains varies from 1.70 to 1.95 Ga [Okrugin et al., 2018, 2020].

The study was aimed at forecasting potential indigenous sources of gold and platinum which form placer and primary deposits of the area. This requires the development of objective mineralogical-geochemical criteria for certain parameters of formation conditions for deep-seated sources of parent ore. The tasks included: 1) determination of chemical composition and content of admixture elements in metabasites and dolerites; 2) identification and characterization of rocks based on the petrographic and geochemical data; 3) analysis of distribution patterns for chemical elements and geochemical indicator ratios of geodynamical settings and sources of the substance; 4) ore mineralization formation model refinement.

## 2. GEOLOGICAL STRUCTURE OF THE STUDY AREA

The outcrops studied are located within the Nimnyr granulite-orthogneissic terrane (Fig. 1). The structural plan of the terrane is determined by the widespread occurrence of granite-gneiss domes. The largest of them – the Timpton dome, – is located in the northern part of the terrane [Duk et al., 1986]. The domal cores are composed of 3.57–1.93 Ga orthogneisses represented by granite-, charnokite- and enderbite-gneisses with amphibolite bodies [Parfenov, Kuzmin, 2001]. The shoulders of the domes are composed of the paragneissic complex represented by two associations of rocks. The first association (Kurumkan sequence) includes quartzites and high-alumina gneisses, protolithically resulted from decomposition of the rocks with Nd-model

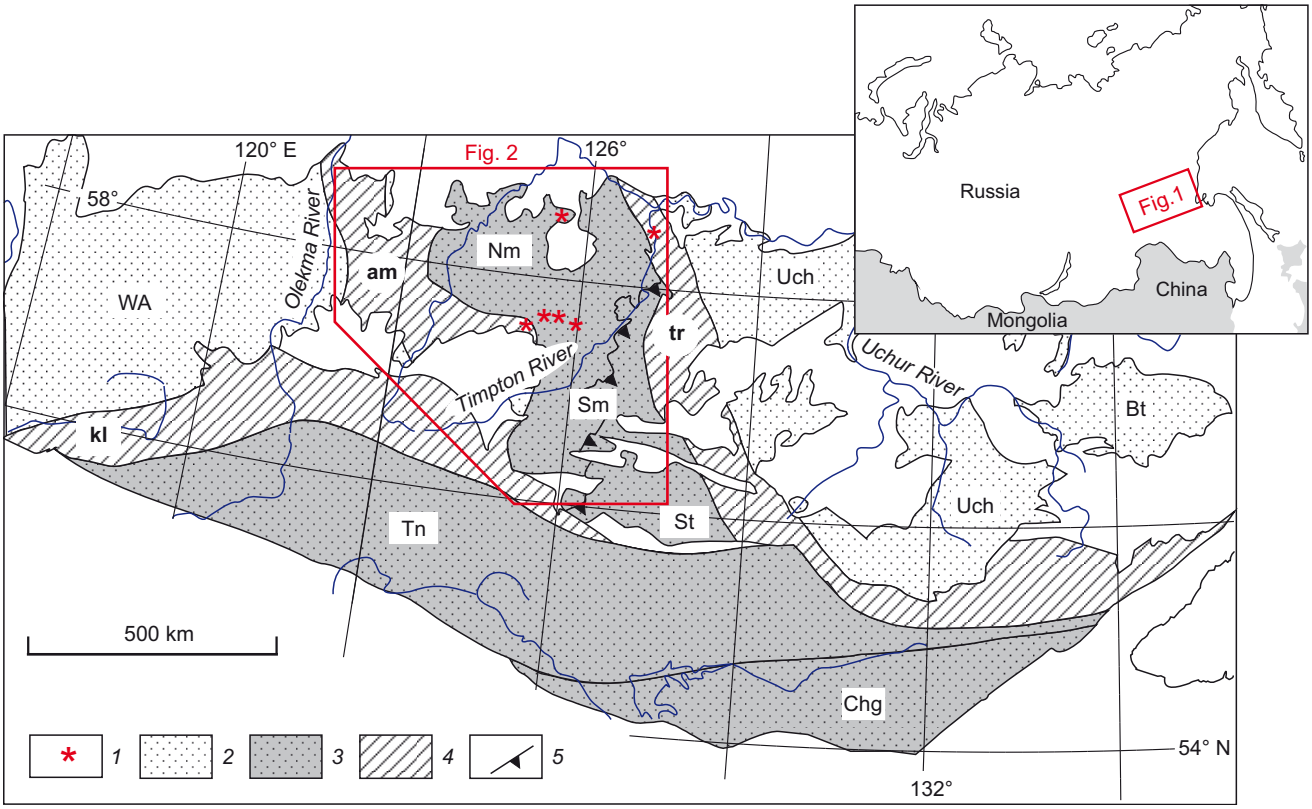


**Fig. 1.** Tectonic scheme of the Aldan–Stanovoy Shield (after [Parfenov, Kuzmin, 2001; Smelov, Timofeev, 2003]), showing the location of the objects studied.

*1* – distribution areas of ore-bearing metabasites and post-ore dolerites; *2* – paleocratonic terranes: WA – West Aldan, Uch – Uchur, Bt – Batomga; *3* – terranes sandwiched between the margins of paleocratons: Nm – Nimnyr, St – Sutam, Tn – Tynda, Chg – Chogar; *4* – zones of tectonic melange: am – Amga, kl – Kalar, tr – Tyrkanda; *5* – Seym thrust (Sm).

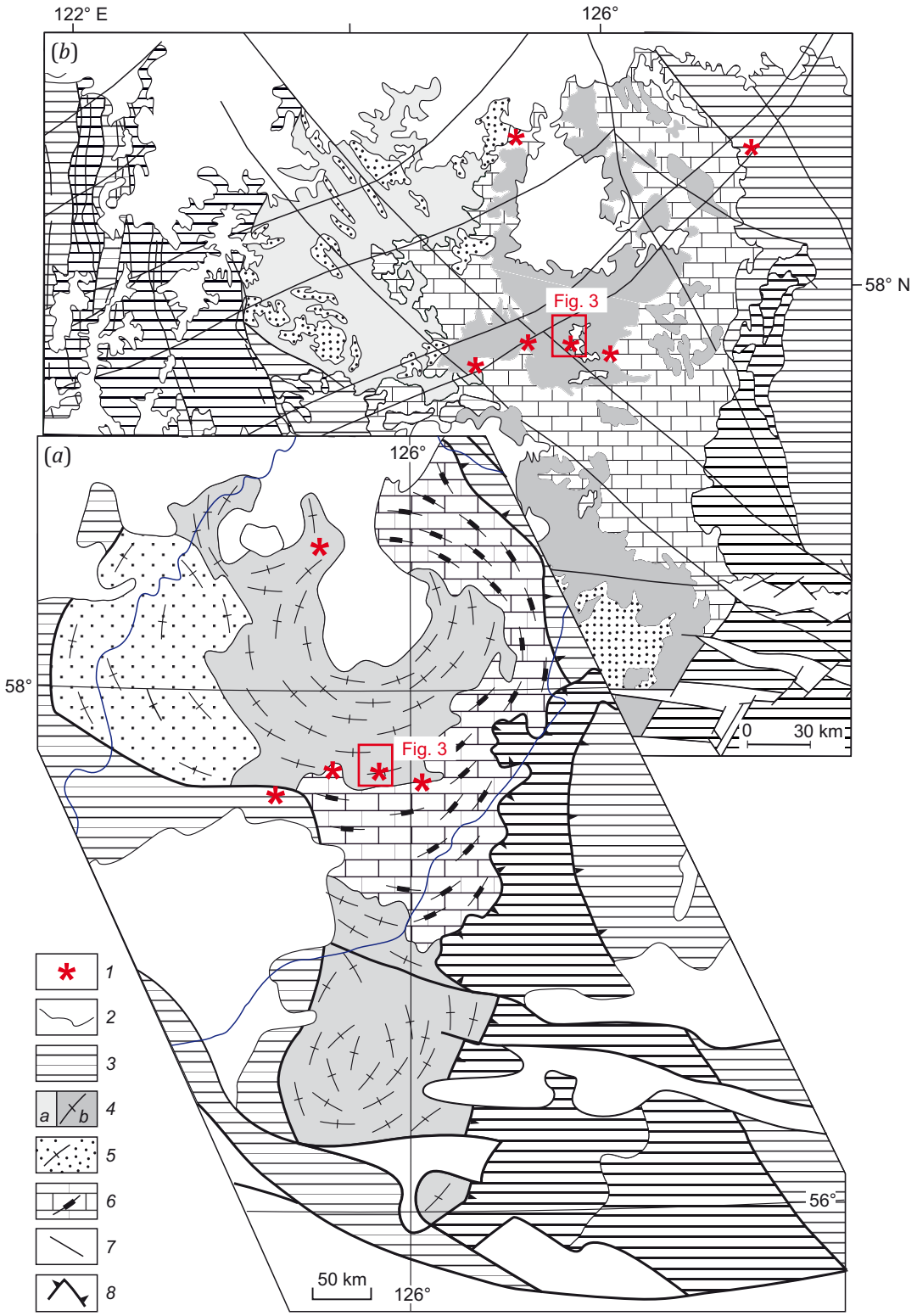


**Fig. 2.** Geological sketch map of the Nimnyr terrane area: (*a*) – [Parfenov, Kuzmin, 2001]; (*b*) – [Velikoslavinskii et al., 2011], simplified. Rock distribution areas: *1* – ore-bearing mafic rocks, *2* – sedimentary cover of the Siberian platform, *3* – complexes outside the Nimnyr terrane, *4* – tonalite-trondhjemite orthogneisses (enderbite-gneisses) of the Western Aldan (a) and Timpton (b) complexes, granite-gneisses, *5* – biotite ± garnet, cordierite, sillimanite plagiogneisses, bipyroxene- and diopside-hornblende crystalline schists of the Kurumkan and other sequences, *6* – hornblende ± biotite, diopside, hypersthene plagiogneisses, hypersthene-biotite plagiogneisses and crystalline schists with rare interlayers of calciphyres of the Fedorovka sequence, *7* – faults, *8* – thrusts.

age of 3.06–2.85 Ga [Parfenov, Kuzmin, 2001], as well as calcareous and ferruginous quartzite lenses [Rundqvist, Mitrofanov, 1988; Duk et al., 1986]. The second association (Fedorovka sequence) is represented by 2006 Ma amphibole, biotite-amphibole, diopside-amphibole and bipyroxene-amphibole plagiogneisses [Velikoslavinsky et al., 2006], less often by schists with interlayers and lenses of diopside and phlogopite-diopside rocks and calciphyres [Parfenov, Kuzmin, 2001] (Fig. 2).

Gold mineralization in the terrane is localized in extended metabasite bodies of the Medvedev complex, intruding sub-conformably the orthogneissic complex and metamorphic rocks of the Kurumkan and Fedorovka sequences and constituting combined dikes with 1920 Ma alaskite granites [Shcherbak, Bibikova, 1984; Kravchenko et al., 2009]. The bodies are located in the interdomal synforms (Fig. 3, a). The degree of metamorphism experienced by metabasites and host rocks corresponds to the granulite facies. Among the rocks of the Medvedev complex, the most common are bipyroxene-amphibole and pyroxene-amphibole crystalline schists; there occur olivine- and pyroxene-containing amphibolites. At some outcrops, the bodies are deformed by asymmetric folds with steep hinges which occur during the shear motions. Where the metamorphic rocks show signs of bending, folding and secondary schistosity in association with sub-conformable quartz veins and pyroxene and amphibole bands and lenses, the crystalline schists contain vein-disseminated metamorphogenic-hydrothermal sulfide-arsenide ores presenting in the Pinigin deposit and some ore fields (Fig. 3, a, b). It suggests the formation of the complex and its related mineralization at the final collisional stage [Smelov et al., 2006; Kravchenko et al., 2010]. The $^{40}Ar/^{39}Ar$ age of metamorphism of the rocks from the Medvedev complex, determined based on the amphiboles from the bipyroxene-amphibole crystalline schist and pyroxene-plagioclase-quartz rock in the ore interval, was 1903–1908 Ma [Smelov et al., 2006].

The formation temperature estimation values for bipyroxene and amphibole-plagioclase associations of the

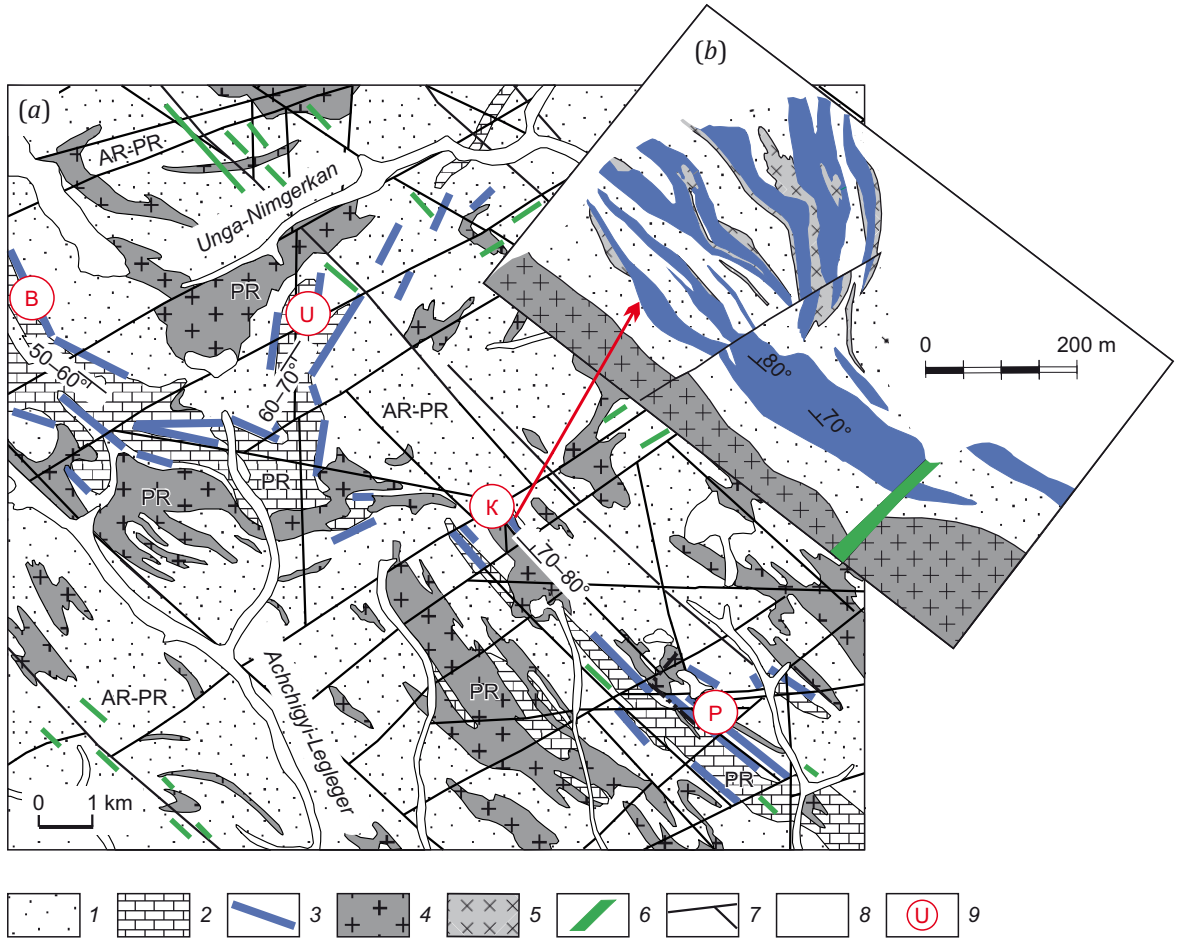


**Fig. 3.** Geological sketch-maps of outcrops of metabasites of the Medvedevsky complex compiled on the basis of [Kiselev et al., 1988]. (*a*) – a fragment of the Leglier ore cluster; (*b*) – a fragment of the Kur section of the Pinigin deposit. *1* – AR-PR metamorphic complexes – biotite-hypersthene and garnet-biotite plagiogneisses of the orthogneissic complex and the Kurumkan sequence; *2–6* – PR metamorphic complexes: *2* – plagiogneisses and crystalline schists of the Fedorovka sequence, *3–6* – PR intrusions: *3* – bodies of rocks of the Medvedev complex, *4* – granites and granite-gneisses, *5* – plagiogranitoids, *6* – dolerites (on the basis of [State Geological Map..., 1962]); *7* – faults; *8* – Quaternary deposits; *9* – areas of orogenic gold mineralization: B – Brivas and U – Unga-Nimgerkan of the Brivas ore field, K – Kur and P – Pritrassovy of the Verkhnelyubkakai ore field.

crystalline schists of the deposits using different geothermometers were 750–850 °C; pressure estimation value based on the amphibole composition was 5–7 kbar [Kravchenko et al., 2010]. Based on the fluid inclusions in plagioclases and pyroxenes, there were obtained the effects of gas emission corresponding to high-temperature (780–480 °C) and moderate-temperature (450–180 °C) ore-forming fluids of the metamorphic and later stages [Sharova, 2006].

The area of occurrence of metabasites of the Medvedev complex includes a zone of intersecting doleritic dikes (Fig. 3), widespread within the Aldan Shield and constituting the E-NE- and NW-extended dike belts [Okrugin et al., 2000, 2019] – Timpton-Gynym (TG) and Timpton-Algamay (TA), with precise U-Pb ages of 1869±2 and 1754 ±5 – 1759±4 Ma [Ernst et al., 2016]. The metabasites of the Medvedev complex and ore bodies are intersected by dolerites (Fig. 3, b). The doleritic dikes are steeply dipping (70–90°), brought into direct, sharply defined transcurrent contacts, extend a few hundred meters to 12–15 km, and vary in thickness from a few tens of meters to 200–300 m. They are unsusceptible to metamorphic transformations, fresh-appearing, and consist of dark-gray and black massive fine- and medium-grained rocks with fine-grained chilled endocontact zones. The rocks have ophitic and gabbro-ophitic texture; at the endocontacts, they are characterized by microlithic texture. The primary minerals are plagioclase and clinopyroxene, the secondary minerals are K-feldspar, hypersthene, quartz, titanomagnetite, and apatite. There are dioritic dikes characterized by a high content of interstitial quartz-feldspathic micropegmatite and the occurrence of hypersthene. The 1869 Ma dikes were intruded at the post-collisional extension stage, and the 1750 Ma dikes reflect the intraconinental extension stage [Donskaya, Gladkochub, 2021; Gladkochub et al., 2022].

The belonging of metabasites and dolerites to the pre-ore and post-ore magmatic rocks of similar material composition makes them actual for investigation of mineralogical-geochemical features indicating ore genesis processes.

## 3. METHODS AND MATERIALS

On the Pinigin deposit area, eastward to the Sivaki and Korot rivers, westward to the Khair and Khatymi rivers and northward near the Orto-Sala and Seligdar rivers, there were collected 55 rock samples from the Medvedev complex and more than 40 dolerite samples from 8 dikes of the Timpton-Gynym and Timpton-Algamay belts.

Optical properties of minerals and rocks were studied using Meiji Techno 9430L, Olympus Bx50 and Polam-P-211 microscopes. 75 samples were used to determine chemical composition and microelements including REE. The contents of rock-forming oxides were determined by silicate analysis using wet chemical methods at the department of physical and chemical methods of analysis of DPMGI SB RAS (Yakutsk). The rare-earth and rare element contents were analyzed by LA-ICP-MS at the Shared Research Facilities of Multi-Element and Isotope Researches of SB RAS (IGM SB RAS, Novosibirsk). The analytical data were processed using comparative characteristics and discriminant and petrogenetic diagrams drawn by different authors.

## 4. RESULTS

### 4.1. Rock composition in the Medvedev complex

Five groups of rocks within the Medvedev complex can be distinguished according to the petrographic data. The first and the second groups are represented by hornblende-rich amphibolites which also contain some amounts of olivine and pyroxene. Individual samples include spinel and magnetite. A characteristic distinction of the second group of amphibolites is the presence of a small amount of plagioclase. The third-fifth groups of rocks are dominated by pyroxene-amphibole and bipyroxene-amphibole crystalline schists. Some of the schists contain rare ore minerals, titanite, apatite, biotite, and quartz. The fourth and the fifth groups are characterized by the presence of ore minerals and pyroxene. All samples of the fifths group contain clinopyroxene. Gold mineralization is confined to the last two groups. The rocks of the groups in their chemical composition (Table 1; Suppl. 1 on the article page online) are similar to: 1 – peridotites, pyroxenites and hornblendites; 2 – pycrodolerites; 3 – high- and moderate-Mg dolerites; 4 – low-Mg dolerites; 5 – (high-ferriferous) dolerites.

The non-metamorphosed post-ore doleritic dikes possess homogeneous structures with no visible signs of differentiation. However, they differ from each other in chemical composition (Table 1; Suppl. 1 on the article page online). An important discriminant feature is Ti- and P-contents relative to alkalinity and $SiO_2$-content [Okrugin et al., 2000]. According to this, the dikes are divided into two groups – Ti- ($TiO_2$ more than 1.5 wt. %) and low-Ti ($TiO_2$ less 1.5 wt. %) [Okrugin et al., 2000, 2019].

A feature common to the rocks the Medvedev complex or dolerites is that they belong to the normal range of alkalinity and tholeiitic series (Fig. 4, a–c). In terms of rock-forming oxide content, there is no overlap in composition between the metabasites of groups 1–3 and dolerites; the metabasites of groups 4-5 are similar to Ti-dolerites (Fig. 4, a–d). The points of low-Ti- and Ti-dolerites and NW- and NE-trending belts in Fig. 4 coincide with each other, i.e., there is no difference between these belts. Ti-dolerites are characterized by a high content of $P_2O_5$ (0.2–0.5 wt. %); a similar trend is also seen for the change in $TiO_2$ and $P_2O_5$ contents depending on silica content in the rocks (Fig. 4, d). Low-Ti dolerites with a high $SiO_2$ content show a gradual increase in Ti- and P-contents while Ti-dolerites exhibit abrupt rather than gradual decrease in the content of these elements. This duality of titanium and phosphorus behavior may be attributed to fractional differentiation of basite melts in deep-seated chambers. Thus, the dolerites exhibit only geochemical (low-Ti and Ti) characteristics which probably resulted from differentiation of basites in the intermediate sources with no dependency on the age of different-trending dike belts.

Spectral distribution of elements on the spider diagram shows that the metabasites of groups 1–3 are similar

**Table 1.** Average chemical compositions (wt. %) and content of rare elements (ppm) in the rocks of the Medvedev complex and dolerites

| Components | Rocks of the Medvedev complex | | | | | TG – dolerite belt | | TA – dolerite belt | |
|---|---|---|---|---|---|---|---|---|---|
| | 1 | 2 | 3 | 4 | 5 | 6 | 7 | 8 | 9 |
| $SiO_2$ | 44.45 | 44.00 | 44.82 | 46.78 | 48.82 | 53.55 | 48.48 | 52.24 | 53.46 |
| $TiO_2$ | 1.14 | 1.86 | 2.08 | 2.27 | 2.78 | 0.76 | 2.65 | 0.89 | 1.11 |
| $Al_2O_3$ | 7.50 | 8.96 | 12.16 | 12.73 | 13.34 | 16.80 | 13.57 | 14.54 | 14.72 |
| $Fe_2O_3$ | 3.80 | 4.81 | 4.62 | 3.85 | 4.59 | 0.49 | 3.97 | 2.51 | 2.76 |
| FeO | 9.28 | 10.55 | 10.29 | 11.86 | 10.72 | 10.12 | 11.12 | 9.63 | 7.07 |
| MnO | 0.21 | 0.22 | 0.22 | 0.25 | 0.26 | 0.39 | 0.20 | 0.18 | 0.15 |
| MgO | 21.31 | 15.59 | 10.16 | 6.81 | 4.57 | 2.87 | 5.10 | 5.55 | 5.93 |
| CaO | 8.95 | 10.01 | 11.16 | 11.04 | 9.64 | 8.86 | 8.07 | 9.21 | 9.31 |
| $Na_2O$ | 0.62 | 1.42 | 2.03 | 2.14 | 3.23 | 2.76 | 1.71 | 2.67 | 2.27 |
| $K_2O$ | 0.31 | 0.45 | 0.69 | 0.69 | 0.62 | 2.16 | 0.64 | 1.25 | 1.02 |
| $P_2O_5$ | 0.12 | 0.13 | 0.20 | 0.20 | 0.31 | 0.18 | 0.52 | 0.12 | 0.15 |
| $H_2O$ | 1.43 | 0.76 | 0.56 | 0.23 | 0.62 | – | – | – | – |
| LOI | 0.89 | 1.06 | 0.51 | 0.96 | 0.32 | 0.43 | 3.68 | 0.13 | 1.63 |
| Total | 100.01 | 99.81 | 99.50 | 99.81 | 99.80 | 99.37 | 99.71 | 98.92 | 99.56 |
| La | 9.63 | 14.62 | 19.87 | 20.05 | 21.05 | 34.32 | 36.79 | 20.40 | 25.16 |
| Ce | 22.82 | 38.69 | 51.00 | 46.99 | 46.07 | 74.69 | 80.13 | 40.42 | 50.12 |
| Pr | 3.03 | 4.75 | 7.67 | 6.48 | 6.20 | 9.47 | 9.30 | 4.75 | 6.19 |
| Nd | 13.37 | 21.21 | 33.16 | 28.07 | 27.56 | 41.41 | 38.87 | 19.76 | 25.85 |
| Sm | 3.47 | 5.50 | 7.20 | 7.10 | 7.17 | 7.27 | 7.27 | 3.63 | 4.75 |
| Eu | 0.95 | 1.45 | 2.15 | 2.02 | 2.18 | 1.92 | 2.10 | 1.07 | 1.32 |
| Gd | 3.45 | 5.54 | 6.44 | 7.30 | 7.82 | 7.25 | 7.37 | 3.76 | 4.67 |
| Tb | 0.51 | 0.84 | 0.89 | 1.12 | 1.18 | 0.97 | 1.15 | 0.58 | 0.65 |
| Dy | 3.03 | 4.91 | 4.82 | 6.68 | 7.43 | 5.86 | 6.20 | 3.59 | 3.90 |
| Ho | 0.58 | 0.94 | 0.90 | 1.32 | 1.52 | 1.08 | 1.33 | 0.73 | 0.77 |
| Er | 1.64 | 2.58 | 2.34 | 3.73 | 4.31 | 3.06 | 3.76 | 2.11 | 2.09 |
| Tm | 0.22 | 0.34 | 0.31 | 0.51 | 0.61 | 0.42 | 0.51 | 0.31 | 0.30 |
| Yb | 1.43 | 2.09 | 1.93 | 3.33 | 4.07 | 2.58 | 3.11 | 2.04 | 1.97 |
| Lu | 0.20 | 0.29 | 0.27 | 0.47 | 0.58 | 0.40 | 0.45 | 0.31 | 0.28 |
| Rb | 8.63 | 10.44 | 15.99 | 15.03 | 11.03 | 32.90 | 35.06 | 33.51 | 18.24 |
| Sr | 98.13 | 88.2 | 288.7 | 264.7 | 295.5 | 514.6 | 348.2 | 245.69 | 324.93 |
| Y | 15.37 | 23.86 | 22.28 | 33.97 | 40.26 | 31.45 | 35.71 | 20.11 | 20.99 |
| Zr | 80.33 | 102.0 | 124.81 | 123 | 199 | 222.08 | 232.9 | 117.2 | 139.5 |
| Nb | 7.08 | 12.47 | 15.62 | 15.05 | 17.96 | 12.02 | 14.51 | 5.52 | 8.19 |
| Ba | 73.6 | 100.7 | 331.7 | 214.3 | 226.3 | 730.47 | 518.5 | 455.51 | 367 |
| Hf | 2.15 | 2.62 | 3.34 | 3.45 | 5.08 | 5.31 | 5.61 | 3.24 | 3.60 |
| Ta | 0.43 | 0.58 | 0.79 | 0.96 | 1.08 | 0.70 | 0.86 | 0.39 | 0.50 |
| Th | 0.94 | 1.24 | 1.51 | 4.12 | 0.99 | 3.04 | 4.65 | 5.20 | 3.57 |
| U | 0.31 | 0.49 | 1.00 | 0.66 | 0.69 | 0.63 | 0.92 | 1.33 | 0.57 |
| Cs | 1.24 | 0.73 | 0.71 | 1.11 | 0.19 | 0.47 | 0.64 | 0.62 | 0.30 |
| V | 240 | 289.4 | 347.8 | 368.4 | 366.3 | 402.0 | 368.0 | 248.0 | 278.0 |
| Co | 83.74 | 74.76 | 58.40 | 52.58 | 38.61 | 67.8 | 54.6 | 37.60 | 38.40 |
| Cr | 1958.8 | 1135 | 645.8 | 157.6 | 135.2 | 50.4 | 17.0 | 18.0 | 21.7 |
| Ni | 1007.8 | 588.8 | 260.38 | 108.2 | 71.77 | 54.6 | 73.0 | 76.0 | 62.3 |
| Gd/Yb | 2.41 | 2.65 | 3.34 | 2.19 | 1.92 | 2.81 | 2.37 | 1.84 | 2.37 |
| Dy/Yb | 2.11 | 2.34 | 2.50 | 2.01 | 1.82 | 2.27 | 1.99 | 1.75 | 1.98 |

Note. 1–5 – average compositions for groups of rocks of the Medvedev complex: 1–2 – amphibolites with MgO 29–18 and 18–12 %; 3–5 – crystalline schists with MgO 12–8, 8–6 and 6–4 %. 6–7, 8–9 – average compositions of low-Ti and Ti-dolerites from the Timpton-Algamai and Timpton-Gynym dike belts. * – rocks accompanying gold mineralization.

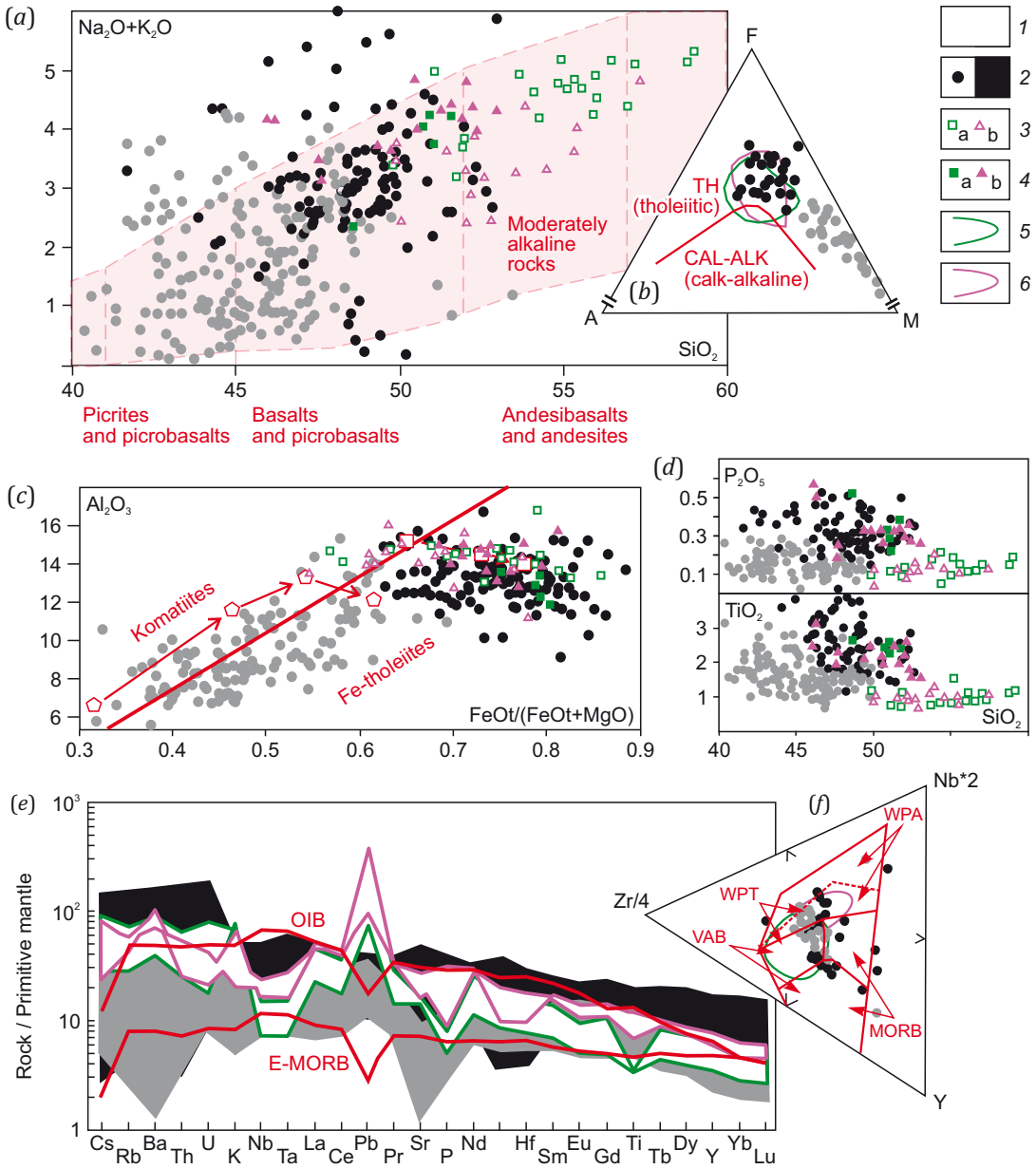


**Fig. 4.** The most pronounced geochemical characteristics of rocks on the diagrams [Petrographic Code..., 2008; Nesbitt et al., 1979; Meschede, 1986].

*1–2* – points and fields of composition of rocks of the Medvedev complex by rock groups: *1* – first-third, *2* – fourth-fifth; *3–4* – points of dolerite compositions: *3* – compositions of low-Ti dolerites from the NE- (a) and NW-trending (b) dike belts; *4* – the same applies for Ti-dolerites; *5–6* – fields of low-Ti- (*5*) and Ti-dolerite (*6*) compositions. Normalization is done after [Sun, McDonough, 1989]. The line on the AFM diagram is drawn after [Irvine, Baragar, 1971]. Discrimination characteristics are shown in red.

to enriched mid-ocean ridge basalts and those of groups 4–5– to intraplate ocean island basalts. Unlike the latter, the dolerites are characterized by the presence of well-defined negative Th-U, Nb-Ta, Zr-Hf, P and Ti anomalies (Fig. 4, e). In the discriminant diagram, reflecting compositional features of rocks in different geodynamic settings, most of the metabasite and dolerite composition points fall into the fields corresponding to intraplate tholeiites, combined with intraplate alkaline and arc volcano basalts (Fig. 4, f).

Spectral distributions of heavy rare-earth elements are different. It was found that REEs present relatively low contents in metabasites of groups 1–3. With an increase in $Al_2O_3$ content, there is an observable increase in the REE spectral slope (Gd/Yb, Dy/Yb ratios in Table 1) and a change of negative Eu anomalies to positive (Fig. 5, a). These features can be indicative of the process of magmatic differentiation with possible participation of plagioclase. The calculation of rare-earth element contents during the melting of clinopyroxene-rich lherzolites [Lesnov, 2010] using batch melting equation $C_L=C_0/(D_0+F(1-P))$ [Zou, 2007] shows that the REE contents similar to those for groups 1–3 can be obtained on 30, 10 and 1 % melting in these rocks (Fig. 5, d).

More gentle spectral slopes and high rare-earth element contents were found in metabasites of groups 4–5 (Fig. 5, b). The calculation of rare-earth element contents on melting of harzburgites [Lesnov, 2010] shows that the REE distribution similar to that in groups 4 and 5 will most likely be obtained by 1 and 10 % melting in these rocks (Fig. 5, e). The calculations of the REE contents on melting of garnet lherzolites show other spectra, though high heavy REE contents could be attributed to the presence of garnet [Lesnov, 2012]. The negative and positive Eu anomalies are probably caused by the process of magmatic fractionation.

Dolerites show HREE concentrations comparable to those in metabasites but higher LREE concentrations (Fig. 5, c). This can be related to the participation of an enriched mantle source in the initial melt formation. There were detected weak negative Eu anomalies. The low-Ti dolerites exhibit a more gently sloping HREE distribution pattern (Gd/Yb, Dy/Yb ratios in Table 1).

The influence of different degrees of melting of the mantle sources on the rock compositions can be seen in diagrams (Fig. 5, f, g). Flat HREE distribution patterns of rocks in these diagrams are confined to the fields reflecting a higher melting degree.

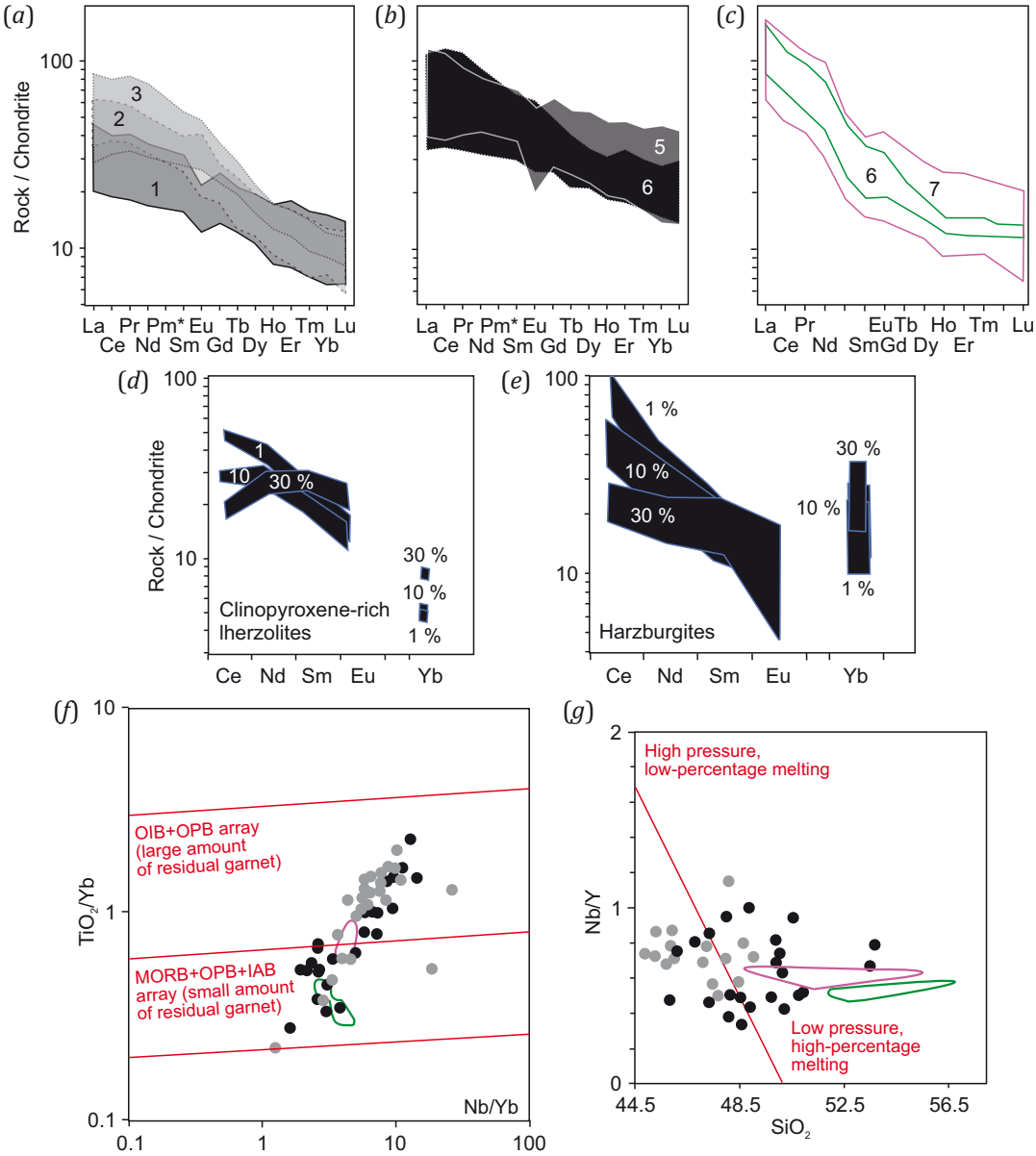


**Fig. 5.** Distribution of rare-earth elements and melting degrees of sources.
(*a–c*) – chondrite-normalized contents of rare earth elements after [Sun, McDonough, 1989]: 1–5 – for metabasites of the groups considered; 6–7 – for low- and high-Ti dolerites; (*d*, *e*) – contents of rare earth elements calculated for batch melting of lherzolites and harzburgites. The calculations were made using the parameters presented in [Johnson et al., 1990], 1 % melting is largely observed in pyroxenes, 30 % melting – in spinel and olivine. Normalization was performed after [Sun, McDonough, 1989]; (*f*, *g*) – element ratios reflecting source melting features: OIB – basalts of oceanic islands, OPB – oceanic plateaus, MORB – mid-oceanic ridge, IAB – island arcs [Pearce et al., 2021; Greenough, McDivitt, 2018]. See Fig. 4 for the legend.

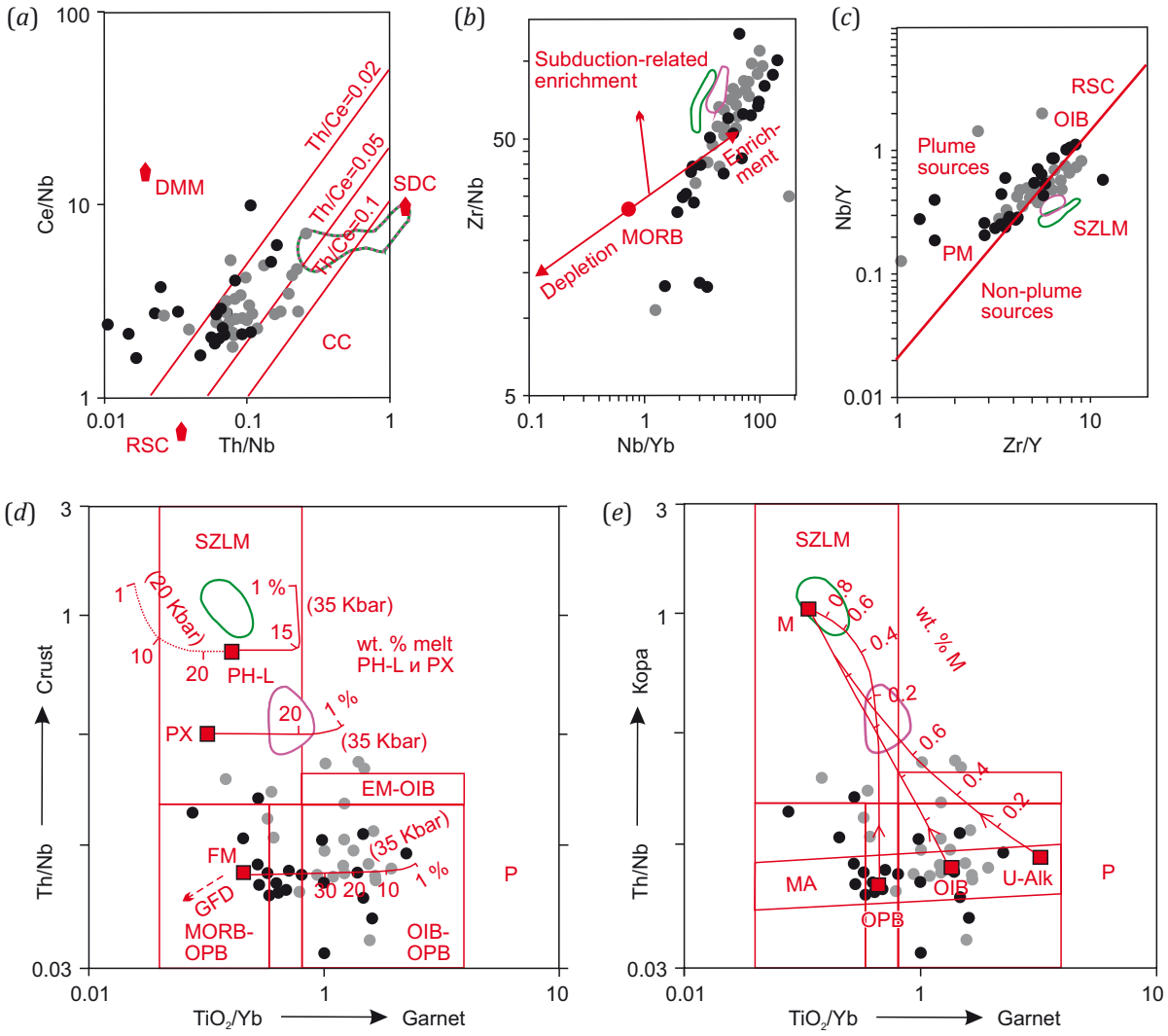


**Fig. 6.** Probable sources of the substance (diagrams after [Saunders et al., 1988; Pearce, 2008; Condie, 2005; Pearce et al., 2021]). DMM – depleted mantle; RSC – recycled component; SDC – subduction component; OIB – oceanic island basalts; PM – primitive mantle; SZLM – subduction zone lithospheric mantle; PH-L – melting trend of phlogopite and lherzolite; PX – pyroxenite melting trend, FM – enriched mantle, GFD – depletion trend in granulite facies, M – SZLM magma, MA – asthenosphere, P – plume.

The analysis of the diagrams reflecting the source types shows that the enrichment of metabasites and dolerites in rare and rare-earth elements is of a different nature. The metabasites are characterized by geochemical markers related to non-subduction, probably plume component, and the dolerites – by the markers related to subduction-enriched lithospheric mantle (Fig. 6, a–e). During the initial melt formation the protoliths of the rocks from the Medvedev complex were presumably derived from different-degree mantle melting and plume-lithosphere interaction which is evidenced by the point distributions along melting and assimilation trends in Fig. 6, d, e.

### 4.2. Material composition of ores

The associations of ore minerals in metabasites are related to magmatic, metamorphic and hydrothermal processes. There were found the relics of magmatic pentlandite-chalcopyrite-pyrrhotite ores having an association of cubic chalcopyrite – hexagonal nickel-bearing pyrrhotite with decay structures (Fig. 7, a). Metamorphogenic pyrrhotite (without decay structures), chalcopyrite, arsenopyrite and loellengite were found with pyroxenes, hornblende, and plagioclase (Fig. 7, b–d). The shape of the above-mentioned mineral grains reflects the structural-balance (Fig. 7, b) and induction (Fig. 7, d) joint growth boundaries typical of metamorphogenic structures. The content of gold (admixture form) in loellingite is up to 200 ppm. The replacement of rock-forming minerals by biotite, actinolite, chlorite, quartz veinlets and rare K-feldspar grains is associated with hydrothermal generation of pyrrhotite and arsenopyriye (Fig. 7, e–i). The latter are represented by homogenous small grains occurring in bunches and veinlets. Arsenopyrite occurs as idiomorphic crystals in hydrothermal association of ore minerals together with pyrrhotite and chalcopyrite, forming either single grains or small aggregates. Cobaltite and isolated occurrences of native gold precipitation form rims around loellingite (Fig. 7, f). A microprobe analysis showed the presence of bismuth

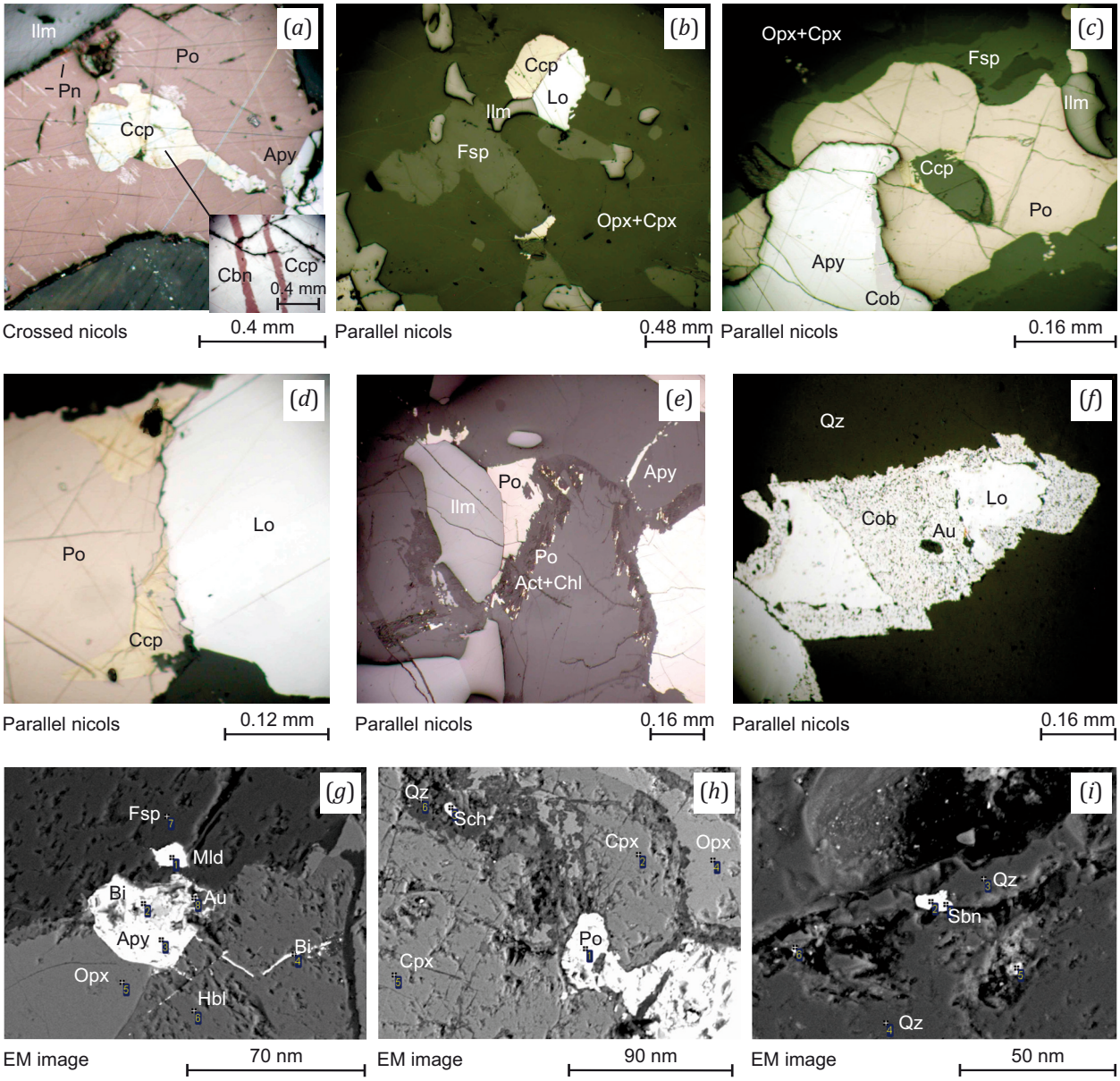


**Fig. 7.** Micrographs of metamorphogenic-hydrothermal ores in metabasites of the Pinigin deposit.
(*a*) – relic magmatogenic ores – lamellar particles of pentlandite and cubanite in pyrrhotite and chalcopyrite, respectively; (*b–d*) – disseminated metamorphogenic ores: (*b*) – structural-balance boundaries of chalcopyrite, ilmenite and loellingite, (*c*) – discontinuous rim of cobaltite at the pyrrhotite-arsenopyrite boundary, (*d*) – loellingite and pyrrhotite joint-growth induction boundary; (*e–i*) veinlet-disseminated hydrothermal ores: (*e*) – distribution of hydrothermal pyrrhotite-2 and arsenides along small fissures and rims of primary silicates together with chlorite and actinolite, (*f*) – particle of native gold at the loellingite-cobaltite boundary, (*g*) – distribution of arsenopyrite-2, bismuth and gold along small fissures and boundaries in rock-forming minerals, (*h*) – scheelite and pyrrhotite inclusions in a quartz veinlet, (*i*) – stibnite inclusion in a quartz veinlet. Mineral abbreviations after [Whitney, Evans, 2010]: Act – actinolite, Apy – arsenopyrite, Au – native gold, Bi – native bismuth, Ccp – chalcopyrite, Cob – cobaltite, Fsp – plagioclase, Hbl – hornblende, Ilm – ilmenite, Lo – loellingite, Mld – maldonite, Opx – orthopyroxene, Po – pyrrhotite, Sch – scheelite, Sbn – stibnite, Qz – quartz.

and tellurium minerals, as well as of stibnite and scheelite (Fig. 7, g–i).

## 5. DISCUSSION

In terms of formation conditions and set of wall-rocks and ores, ore mineralization in metabasites of the Medvedev complex can be compared with hypozonal orogenic gold deposits (Fig. 8, a, b). Such deposits are characterized by the early ore stage dominated by pyrrhotite, arsenopyrite, and loellingite. It is followed by the late ore stage which comprises gold, non-precious metals, and Bi-containing minerals. Mineral ore deposits form at ~4.0–5.5 kbar and 450–550 °C [Groves et al., 2020a; Zhao et al., 2022; Li et al., 2022]. This type of deposits is usually characterized by the ore-forming fluid source problem [Fu, Touret, 2014; Phillips, Powell, 2009] (Fig. 8, b). The approach to solving this problem traditionally emphasizes subduction processes (Fig. 8, c); an alternative model is

related to the asthenospheric upwelling and reactivation of the ancient enriched lithospheric mantle [Groves et al., 2020a] (Fig. 8, d).

The culmination accretionary-collisional, metamorphic and magmatic events in the central Aldan Stanovoy Shield are confined to the Paleoproterozoic (2.01–1.87 Ga) [Kotov, 2003; Donskaya, 2020; Smelov, Timofeev, 2007]. From 2011±2 to 2006±3 Ma, there was an initiation of the Fedorov island arc and formation of volcanic rocks of the Fedorovka sequence. 1993±1 Ma is associated with the formation of the Chuga and Fedorovka thrust faults as a result of the collision between the Fedorovka volcanic arc and the Olekma-Aldan continental microplate [Velikoslavinsky et al., 2006; Kotov, 2003; Anisimova, 2007]; 1.97–1.95 Ga – with the formation of granite intrusions and leucogranites of the Dzhaltundin complex which are post-collisional relative to the collision of the Fedorovka island arc [Kotov, 2003].

It is probable that the formation of the subduction-enriched lithospheric mantle is related to the Fedorovka rock sequence development and occurred prior to the formation of rocks of the Medvedev complex.

The time interval of 1.95–1.92 Ga for the Nimnyr terrane is characterized by the eastward-observed formation of an active margin of the Olekma-Aldan continental microplate and the accumulation of volcano-sedimentary sequences east of the terrane [Kotov, 2003]. Based on the study of xenoliths from the Precambrian metamorphic complexes in the Mesozoic intrusives, 1.96–1.90 Ga terrane is presumably associated with magmatic underplating [Kravchenko et al., 2012]. This age overlaps with the intrusion [Kravchenko et al., 2009] of 1.92 Ga dikes of the Medvedev complex and 1.91–1.90 Ga metamorphism. Metamorphism is characterized by the isothermal decompression trend [Smelov, 1996]. 1.87 Ga ago there was the formation of granite intrusions of the Kodar complex, most likely corresponding to the final stages of the processes during collision of the Aldan and Dzhugdzhur-Stanovoi continental plates [Kotov, 2003], and post-collisional dolerite intrusion.

Ore formation in the rocks of the Medvedev complex lasted from 1.92 to 1.87 Ga. There is no evidence for subduction during this interval; it is characterized by intrusion and metamorphism of pre-ore basites of the Medvedev

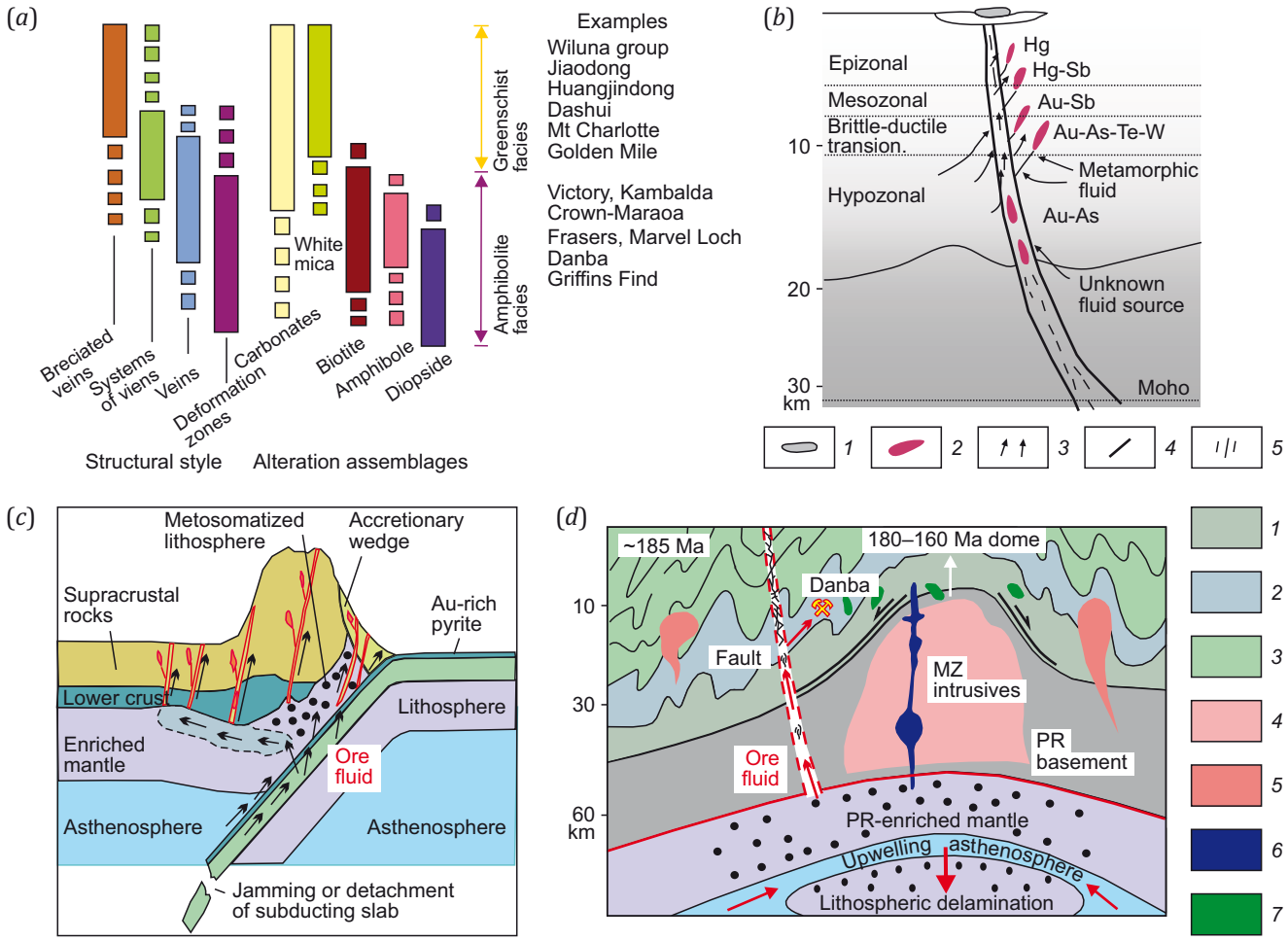


**Fig. 8.** Model for the formation of hypozonal orogenic gold deposits (after [Groves et al., 2020a, 2020b; Zhao et al., 2022]).
(*a*) – conditions and features of metamorphism; (*b*) – ore substance sources; (*c*, *d*) – geological structures. (*b*): *1* – hot spring; *2* – orogenic gold deposits; *3* – fluid flow; *4* – deep-seated fault; *5* – deep-seated fault deformation zone. (*d*): *1* – granulite facies; *2* – amphibolite facies; *3* – greenschist facies; *4* – migmatites / granite gneisses; *5* – MZ granites; *6* – basic magma; *7* – dolerites.

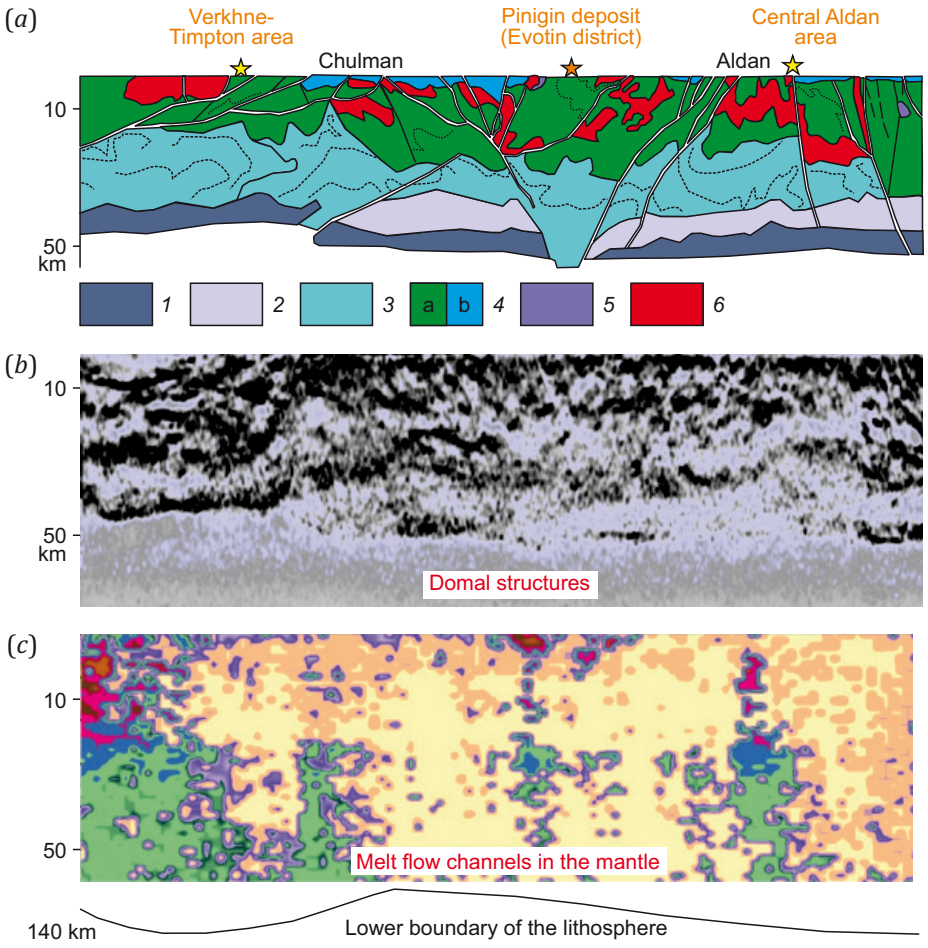


**Fig 9.** Geological-geophysical (*a*) [Kheraskova et al., 2018, simplified] and geophysical (*b*, *c*) [Goshko et al., 2015; Podgorny, Malyshev, 2006] sections along profile 3-DV.
(*a*): *1* – layer 1 – lower crust, heterogeneous, partially melted with ultramafic rocks; *2* – layer 2 – upper crust, metamorphosed mafic-ultramafic rocks; *3* – layer 3 – upper crust, basic rocks with plastic flow traces formed as a result of mantle diapirism; *4* – layer 4 – upper crust, metamorphic rocks with sedimentary cover; *5* – undissected gabbro; *6* – undissected granites and syenites. The line beneath the sections is the lower boundary of the lithosphere.

complex and formation of post-ore non-metamorphosed doleritic dikes. During the same interval, the metamorphic complexes were probably brought to higher levels. The above-described geochemical features of plume activity and enriched lithospheric mantle melting, as well as the features of melt assimilation, mean there is a probability of the plume-lithosphere interaction and ore material activation. The features revealed for the compositions of the mantle magmatic complexes are more suitable for the model shown in Fig. 8, d. Geophysical field imaging of domal structures of the Nimnyr terrane (Fig. 9 a, b) and melt flow channels in the mantle (Fig. 9, c) confirm the adequacy of this model.

Attention is also drawn to a widespread occurrence of placer sperrylite and platinum whose mineralogical-geochemical features are indicative of potential platinum-metal mineralization in this area, which does not exclude the possibility of the Paleoproterozoic complex precious metal deposition.

Multiple mantle magmatic complexes and complex geological structure of the study area necessitate further investigation of mantle events to specify mechanisms and models of ore formation. A more accurate characteristic of sources and geodynamic processes requires the representative isotope-geochemical and isotope-geochronological studies.

## 6. CONCLUSION

The compositional features of pre-ore and post-ore mantle magmatic complexes imply that the most probable source of the Paleoproterozoic ore-forming fluids in the Nimnyr terrane was the ancient subduction-enriched lithospheric mantle interacting with the asthenospheric material. The metamorphic complex formation and its related mineralization occurred at the final collisional stage which favored concentration of ore and its deposition on fold and secondary schistosity sections in metabasites. The period from 1.92 to 1.87 Ga, between formation times of granulite-facies pre-ore basites and post-ore non-metamorphosed dolerites, is likely to be characterized by a significant decrease in the depth of occurrence of metamorphic complexes and by ore formation.

## 7. ACKNOWLEDGEMENTS

The authors are grateful to their colleagues who took part in field and laboratory research, O.M. Turkina and T.V. Donskaya for their comments.

## 8. CONTRIBUTION OF THE AUTHORS

All authors made an equivalent contribution to this article, read and approved the final manuscript.

## 9. DISCLOSURE

The authors declare that they have no conflicts of interest relevant to this manuscript.

## 10. REFERENCES

Anisimova I.V., 2007. Formation Age and Geodynamic Setting of the Greenstone Belts in the Western Aldan Shield. Brief PhD Thesis (Candidate of Geology and Mineralogy). Saint Petersburg, 21 p. (in Russian) [Анисимова И.В. Возраст и геодинамические обстановки формирования зеленокаменных поясов западной части Алданского щита: Автореф. дис. ... канд. геол.-мин. наук. СПб., 2007. 21 с.].

Condie K.C., 2005. High Field Strength Element Ratios in Archean Basalts: A Window to Evolving Sources of Mantle Plumes? Lithos 79 (3–4), 491–504. https://doi.org/10.1016/j.lithos.2004.09.014.

Donskaya T.V., 2020. Assembly of the Siberian Craton: Constraints from Paleoproterozoic Granitoids. Precambrian Research 348, 105869. https://doi.org/10.1016/j.precamres.2020.105869.

Donskaya T.V., Gladkochub D.P., 2021. Post-Collisional Magmatism of 1.88–1.84 Ga in the Southern Siberian Craton: An Overview. Precambrian Research 367, 106447. https://doi.org/10.1016/j.precamres.2021.106447.

Duk V.L., Kitsul V.I., Petrov A.F., Beryozkin V.I., Bogomolova L.M., Smelov A.P., Timofeev V.F., Kovach V.P. et al., 1986. Early Precambrian in Southern Yakutia. Nauka, Moscow, 280 p. (in Russian) [Дук В.Л., Кицул В.И., Петров А.Ф., Берёзкин В.И., Богомолова Л.М., Смелов А.П., Тимофеев В.Ф., Ковач В.П. и др. Ранний докембрий Южной Якутии. М.: Наука, 1986. 280 с.].

Ernst R.E., Hamilton M.A., Söderlund U., Hanes J.A., Gladkochub D.P., Okrugin A.V., Kolotilina T., Mekhonoshin A.S., Bleeker W., LeCheminant A.N., Buchan K.L., Chamberlain K.R., Didenko A.N., 2016. Long-Lived Connection between Southern Siberia and Northern Laurentia in the Proterozoic. Nature Geoscience 9, 464–469. https://doi.org/10.1038/ngeo2700.

Fu B., Touret J.L.R., 2014. From Granulite Fluids to Quartz–Carbonate Megashear Zones: The Gold Rush. Geoscience Frontiers 5 (5), 747–758. https://doi.org/10.1016/j.gsf.2014.03.013.

Gladkochub D.P., Donskaya T.V., Pisarevsky S.A., Ernst R.E., Söderlund U., Kotov A.B., Kovach V.P., Okrugin A.V., 2022. 1.79–1.75 Ga Mafic Magmatism of the Siberian Craton and Late Paleoproterozoic Paleogeography. Precambrian Research 370, 106557. https://doi.org/10.1016/j.precamres.2022.106557.

Goshko E.Y., Efimov A.S., Sal'nikov A.S., 2015. The Recent Structure and the Assumed History of Formation of the Crust in the South-Eastern Segment of the North Asian Craton along Reference Profile 3-DV. Geodynamics & Tectonophysics 5 (3), 785–798 (in Russian) [Гошко Е.Ю., Ефимов А.С., Сальников А.С. Современная структура и предполагаемая история формирования земной коры юго-востока Северо-Азиатского кратона вдоль опорного профиля 3-ДВ // Геодинамика и тектонофизика. 2014. Т. 5. № 3. С. 785–798]. https://doi.org/10.5800/GT-2014-5-3-0155.

Greenough J.D., McDivitt J.A., 2018. Earth's Evolving Subcontinental Lithospheric Mantle: Inferences from LIP Continental Flood Basalt Geochemistry. International Journal of Earth Sciences 107, 787–810. https://doi.org/10.1007/s00531-017-1493-6.

Groves D.I., Santosh M., Deng J., Wang Q., Yang L., Zhang L., 2020a. A Holistic Model for the Origin of Orogenic Gold Deposits and Its Implications for Exploration. Mineralium Deposita 55, 275–292. https://doi.org/10.1007/s00126-019-00877-5.

Groves D.I., Santosh M., Zhang L., 2020b. A Scale-Integrated Exploration Model for Orogenic Gold Deposits Based on a Mineral System Approach. Geoscience Frontiers 11 (3), 719–738. https://doi.org/10.1016/j.gsf.2019.12.007.

Irvine T.N., Baragar W.R.A., 1971. A Guide to the Chemical Classification of the Common Volcanic Rocks. Canadian Journal of Earth Sciences 8 (5), 523–547. https://doi.org/10.1139/e71-055.

Johnson K.T.M., Dick H.J.B., Shimizu N., 1990. Melting in the Oceanic Upper Mantle: An Ion Microprobe Study of Diopsides in Abyssal Peridotites. Journal of Geophysical Research: Solid Earth 95 (B3), 2661–2678. https://doi.org/10.1029/JB095iB03p02661.

Kheraskova T.N., Yakovlev D.V., Pimanova N.N., Berezner O.S., 2018. Conjugation with the Central Asian Foldbelt: Interpretation of the 3DV and Tynda–Amurzet Transects. Geotectonics 52, 1–21. https://doi.org/10.1134/S0016852118010089.

Kiselev G.N. et al., 1988. Report on the Results of Additional Exploration of the South Aldan Iron Ore District. Scale 1:50000. Sheets O-51-83-B, Г; O-51-84-B, Г; O-51-93-93 Б, Г; O-51-94-A, Б, B, Г; O-51-95-A, Б, B, Г; O-51-96-A, Б, B, Г. Report on the Results of the Evota Crew Activities in 1978–1988. Geological Expedition South Yakutia, Chulman (in Russian) [Киселев Г.Н. и др. Отчет о геологическом доизучении площади Южно-Алданского железорудного района в масштабе 1:50000 на листах O-51-83-B, Г; O-51-84-B, Г; O-51-93-93 Б, Г; O-51-94-A, Б, B, Г; O-51-95-A, Б, B, Г; O-51-96-A, Б, B, Г. Отчет по результатам работ Эвотинской партии за 1978–1988 гг. Чульман: ЮЯГРЭ, 1988].

Kotov A.B., 2003. Boundary Conditions of Geodynamic Models for the Continental Crust Growth in the Aldan Shield. Brief PhD Thesis (Doctor of Geology and Mineralogy). Saint Petersburg, 78 p. (in Russian) [Котов А.Б. Граничные условия геодинамических моделей формирования континентальной коры Алданского щита: Автореф. дис. ... докт. геол.-мин. наук. СПб., 2003. 78 с.].

Kravchenko A.A., Smelov A.P., Berezkin V.I., Dobretsov V.N., 2009. Effect of the Magma Mixing Processes on the Composition and Ore Potential of the Medvedevsk Complex Metabasites, the Aldan Shield. National Geology 5, 56–65 (in Russian) [Кравченко А.А., Смелов А.П., Березкин В.И., Добрецов В.Н. Влияние процессов взаимодействия магм на состав и рудоносность метабазитов медведевского комплекса (Алдано-Становой щит) // Отечественная геология. 2009. № 5. С. 56–65].

Kravchenko A.A., Smelov A.P., Beryozkin V.I., Popov N.V., 2010. Geology and Genesis of the Precambrian Gold-Bearing Metabasites in the Central Aldan-Stanovoy Shield (Using the Pinigin Deposit as an Example). Ofset, Yakusk, 148 p. (in Russian) [Кравченко А.А., Смелов А.П., Березкин В.И., Попов Н.В. Геология и генезис докембрийских золотоносных метабазитов центральной части Алдано-Станового щита (на примере месторождения им. П. Пинигина). Якутск: Офсет, 2010. 148 с.].

Kravchenko A.A., Smelov A.P., Popov N.V., Zaitsev A.I., Beryozkin V.I., Dobretsov V.N., 2012. First Data on the Composition and Age of the Lower Crust of the Central Part of the Aldan-Stanovoy Shield: Results of Study of Xenoliths from Mesozoic Plutons. In: Craton Formation and Destruction with Special Emphasis on BRICS Cratons. Abstracts of Workshop (July 21–22, 2012, Johannesburg, South Africa). GSSA, Johannesburg, p. 62–63.

Lesnov F.P., 2010. Rare Earth Elements in Ultramafic and Mafic Rocks and Their Minerals. Main Types of Rocks. Rock-Forming Minerals. CRC Press/Balkema, 560 p.

Lesnov F.P., 2012. Rare Earth Elements in Ultramafic and Mafic Rocks and Their Minerals. Minor and Accessory Minerals. CRC Press/Balkema, 300 p.

Li H., Wang Q., Yang L., Dong C., Weng W., Deng J., 2022. Alteration and Mineralization Patterns in Orogenic Gold Deposits: Constraints from Deposit Observation and Thermodynamic Modeling. Chemical Geology 607, 121012. https://doi.org/10.1016/j.chemgeo.2022.121012.

Meschede M., 1986. A Method of Discriminating between Different Types of Mid-Ocean Ridge Basalts and Continental Tholeiites with the Nb-Zr-Y Diagram. Chemical Geology 56 (3–4), 207–218. https://doi.org/10.1016/0009-2541(86)90004-5.

Nesbitt R.W., Sun S.S., Purvis A.C., 1979. Komatiites: Geochemistry and Genesis. Canadian Mineralogist 17, 165–186.

Okrugin A.V., 2000. Platinum-Bearing Placers of the Siberian Platform. Yakutsk Branch of the Publishing House of SB RAS, Yakutsk, 184 p. (in Russian) [Округин А.В. Россыпная платиноносность Сибирской платформы. Якутск: ЯФ Изд-ва СО РАН, 2000. 184 с.].

Okrugin A.V., Ernst R.E., Beryozkin V.I., Popov N.V., 2019. Late Precambrian Mafic Dyke Swarms of the Aldan Shield and Their Importance in Ore-Magmatic Processes. In: Large Igneous Provinces through Earth History: Mantle Plumes, Supercontinents, Climate Change, Metallogeny and Oil-Gas, Planetary Analogues. Abstracts Volume of the 7 International Conference (28 August – 8 September 2019). Publishing House of CSTI, Tomsk, p. 94–95.

Okrugin A.V., Koroleva O.V., Beryozking V.I., 2000. Distribution Characteristics and Compositional Features of the Riphean Basites in the Aldan Shield. In: Petrography on the Boundary of the XXI Century. Materials of the Second All-Russia Petrographic Meeting. Vol. 1. Geoprint, Syktyvkar, p. 150–153 (in Russian) [Округин А.В., Королева О.В., Березкин В.И. Характер распространения и особенности состава рифейских базитов Алданского щита // Петрография на рубеже XXI века: Материалы Второго всероссийского петрографического совещания. Сыктывкар: Геопринт, 2000. Т. I. С. 150–153].

Okrugin A.V., Yakubovich O.V., Ernst R., Druzhinina Zh.Yu., 2018. Platinum-Bearing Placers of Siberian Platform: Mineral Associations and Their Age Characteristics as Indicators of Large Igneous Provinces Manifested in Old Platform. Arctic and Subarctic Natural Resources 3, 36–52 (in Russian) [Округин А.В., Якубович О.В., Эрнст Р., Дружинина Ж.Ю. Платиноносные россыпи Сибирской платформы: минеральные ассоциации и их возрастные характеристики как индикаторы проявления крупных изверженных провинций на древней платформе // Природные ресурсы Арктики и Субарктики. 2018. № 3. С. 36–52]. https://doi.org/10.31242/2618-9712-2018-25-3-36-52.

Okrugin A.V., Yakubovich O.V., Ernst R.E., Druzhinina Zh.Yu., 2020. Platinum-Bearing Placers: Mineral Associations and Their $^{190}$Pt-$^{4}$He and Re-Os Ages, and Potential Links with Large Igneous Provinces in the Siberian Craton. Economic Geology 115 (8), 1835–1853. https://doi.org/10.5382/econgeo.4773.

Parfenov L.M., Kuzmin M.I. (Eds), 2001. Tectonics, Geodynamics and Metallogeny of the Sakha Republic (Yakutia). MAIK Nauka/Interperiodica, Moscow, 571 p. (in Russian) [Тектоника, геодинамика и металлогения территории Республики Саха (Якутия) / Ред. Л.М. Парфенов, М.И. Кузьмин. М.: МАИК «Наука/Интерпериодика», 2001. 571 с.].

Pearce J.A., 2008. Geochemical Fingerprinting of Oceanic Basalts with Applications to Ophiolite Classification and the Search for Archean Oceanic Crust. Lithos 100 (1–4), 14–48. https://doi.org/10.1016/j.lithos.2007.06.016.

Pearce J.A., Ernst R.E., Peate D.W., Rogers C., 2021. LIP Printing: Use of Immobile Element Proxies to Characterize Large Igneous Provinces in the Geologic Record. Lithos 392–393, 106068. https://doi.org/10.1016/j.lithos.2021.106068.

Petrographic Code of Russia: Magmatic, Metamorphic, Metasomatic and Impact Formations, 2008. VSEGEI, Saint Petersburg, 200 p. (in Russian) [Петрографический кодекс России. Магматические, метаморфические, метасоматические, импактные образования. СПб.: ВСЕГЕИ, 2008. 200 с.].

Phillips G.N., Powell R., 2009. Formation of Gold Deposits: Review and Evaluation of the Continuum Model. Earth-Science Reviews 94 (1–4), 1–21. https://doi.org/10.1016/j.earscirev.2009.02.002.

Podgorny V.Ya., Malyshev Yu.F., 2006. Density Structure of the Lithosphere of the Aldan-Stanovoy Shield. Geophysical Journal 28 (1), 68–81 (in Russian) [Подгорный В.Я.,

Малышев Ю.Ф. Плотностное строение литосферы Алдано-Станового щита // Геофизический журнал. 2006. Т. 28. №. 1. С. 68–81].

Rundqvist D.V., Mitrofanov F.P. (Eds), 1988. Precambrian Geology of the USSR. Nauka, Leningrad, 440 p. (in Russian) [Докембрийская геология СССР / Ред. Д.В. Рундквист, Ф.П. Митрофанов. Л.: Наука, 1988. 440 с.].

Saunders A.D., Norry M.J., Tarney J., 1988. Origin of MORB and Chemically-Depleted Mantle Reservoirs: Trace Element Constraints. Journal of Petrology 1, 415–445. https://doi.org/10.1093/petrology/Special_Volume.1.415.

Sharova T.V., 2006. Material Composition and Features of the Genesis of Gold Mineralization in the Precambrian Metamorphites of the Aldan Shield. Proceedings of Higher Educational Establishments. North Caucasus Region. Natural Sciences 4, 102–103 (in Russian) [Шарова Т.В. Вещественный состав и особенности генезиса золотого оруденения в докембрийских метаморфитах Алданского щита // Известия вузов. Северо-Кавказский регион. Естественные науки. 2006. № 4. С. 102–103].

Shcherbak N.P., Bibikova E.V., 1984. Early Precambrian Stratigraphy and Geochronology of the USSR. In: Precambrian Geology. Proceedings of 27th International Geological Congress (August 4–14, 1984, Moscow, USSR). Vol. 5. Nauka, Moscow, p. 3–14 (in Russian) [Щербак Н.П., Бибикова Е.В. Стратиграфия и геохронология раннего докембрия СССР // Геология докембрия: Доклады 27 международного геологического конгресса (4–14 августа 1984 г., Москва, СССР). М.: Наука, 1984. Т. 5. С. 3–14].

Smelov A.P., 1996. Archean and Proterozoic Metamorphism of the Aldan-Stanovoy Shield. Brief PhD Thesis (Doctor of Geology and Mineralogy). Novosibirsk, 33 p. (in Russian) [Смелов А.П. Метаморфизм в архее и протерозое Алдано-Станового щита: Автореф. дис. … докт. геол.-мин. наук. Новосибирск, 1996. 33 с.].

Smelov A.P., Beryozkin V.I., Popov N.V., Kravchenko A.A., Travin A.V., Shaporina M.N., 2006. First Data on the Paleoproterozoic Syncollisional Mafic and Ultramafic Rocks of the Aldan-Stanovoy Shield. Russian Geology and Geophysics 47 (1), 153–165.

Smelov A.P., Timofeev V.F., 2003. Terrane Analysis and the Geodynamic Model of the Formation of the North Asian Craton in the Early Precambrian. Pacific Geology 22 (6), 42–54 (in Russian) [Смелов А.П., Тимофеев В.Ф. Террейновый анализ и геодинамическая модель формирования Северо-Азиатского кратона в раннем докембрии // Тихоокеанская геология. 2003. Т. 22. № 6. С. 42–54].

Smelov A.P., Timofeev V.F., 2007. The Age of the North Asian Cratonic Basement: An Overview. Gondwana Research 12 (3), 279–288. https://doi.org/10.1016/j.gr.2006.10.017.

State Geological Map of the USSR, 1962. Aldan Series. Scale of 1:200000. Sheet O-51-XXIV. Yakutskgeology, Yakutsk (in Russian) [Государственная геологическая карта СССР. Серия Алданская. Масштаб 1:200000. Лист О-51-XXIV. Якутск: Якутскгеология, 1962].

Sun S.-S., McDonough W.F., 1989. Chemical and Isotopic Systematics of Oceanic Basalts: Implications for Mantle Composition and Processes. Geological Society of London Special Publications 42 (1), 313–345. https://doi.org/10.1144/GSL.SP.1989.042.01.19.

Syasko A.A., Grib N.N., Nikitin V.M., 2006. Comparative Characteristics of the Archean Gold Deposits. Science and Education 4, 58–65 (in Russian) [Сясько А.А., Гриб Н.Н., Никитин В.М. Сравнительная характеристика архейских золоторудных месторождений // Наука и образование. 2006. № 4. С. 58–65].

Turchenko S.I., 2021. Metallogeny of Precambrian Stage of the Earth Geological Evolution. Sprinter, Saint Petersburg, 179 p. (in Russian) [Турченко С.И. Металлогения докембрийского этапа развития Земли. СПб.: Спринтер, 2021. 179 с.].

Velikoslavinskii S.D., Kotov A.B., Sal'nikova E.B., Kovach V.P., Larin A.M., Tolmacheva E.V., 2011. Early Precambrian Granite-Gneiss Complexes in the Central Aldan Shield. Petrology 19, 382–398. https://doi.org/10.1134/S0869591111040060.

Velikoslavinsky S.D., Kotov A.B., Sal'nikova E.B., Kovach V.P., Glebovitsky V.A., Zagornaya N.Yu., Yakovleva S.Z., Anisimova I.V., Fedoseenko A.M., Tolmacheva E.V., 2006. Protoliths of the Metamorphic Rocks of the Fedorov Complex, Aldan Shield: Character, Age, and Geodynamic Environments of Origin. Petrology 14, 21–38. https://doi.org/10.1134/S0869591106010036.

Whitney D.L., Evans B.W., 2010. Abbreviations for Names of Rock-Forming Minerals. American Mineralogy 95 (1), 185–187. https://doi.org/10.2138/am.2010.3371.

Zhao H., Wang Q., Groves D.I., Santosh M., Zhang J., Fan T., 2022. Genesis of Orogenic Gold Systems in the Daduhe Belt: Evidence of Long-Lived Fertile Mantle Lithosphere as a Source of Diverse Metallogeny on the Western Margin of the Yangtze Craton, China. Ore Geology Reviews 145, 104861. https://doi.org/10.1016/j.oregeorev.2022.104861.

Zou H., 2007. Quantitative Geochemistry. Imperial College Press, London, 304 p. https://doi.org/10.1142/p444.